Title

Aqueous Photochemistry of 2-Methyltetrol and Erythritol as Sources of Formic Acid and Acetic Acid in the Atmosphere

Journal

ACS Earth and Space Chemistry, 5(6)

ISSN

2472-3452

Authors

Cope, James D

Abellar, Karizza A

Bates, Kelvin H

et al.

Publication Date

2021-06-17

DOI

10.1021/acsearthspacechem.1c00107

Peer reviewed

ACS EARTH AND SPACE CHEMISTRY

http://pubs.acs.org/journal/aesccq

Article

Aqueous Photochemistry of 2-Methyltetrol and Erythritol as Sources of Formic Acid and Acetic Acid in the Atmosphere

James D. Cope, Karizza A. Abellar, Kelvin H. Bates, Xuan Fu, and Tran B. Nguyen*

Cite This: https://doi.org/10.1021/acsearthspacechem.1c00107

Read Online

ACCESS | Metrics & More | Article Recommendations | Supporting Information

ABSTRACT: Atmospheric formic acid (FA) and acetic acid (AA) mixing ratios are often underestimated in atmospheric models, particularly over areas with high biogenic influence. We investigated the aqueous hydroxyl radical (OH) oxidation of 2-methyltetrol, one of the largest components of secondary organic aerosols (SOAs) that are produced from the oxidation of isoprene, and compare its chemistry to the non-methylated C_4 polyol analogue, erythritol. We studied the kinetics and reaction products of the aqueous 2-methyltetrol (2-MT) + OH and erythritol (E) + OH reactions using ^1H and ^{13}C nuclear magnetic resonance spectroscopy and high-performance liquid chromatography coupled with high-resolution mass spectrometry. We found that the aqueous oxidation of aliphatic alcohols, such as E and 2-MT, are strong sources of small acids. Nearly all 2-MT is converted to FA, AA, and carbon dioxide (CO_2) under atmospherically relevant OH exposures. Suppression of volatile acid partitioning into the gas phase increased the observed yields of volatile products in solution by up to 80%, as quantified by experiments with low headspace. The influence of solution pH on the yields of FA and AA (or their carboxylates) was also investigated in the range of pH 2−9 for the 2-MT + OH reaction. Solution pH strongly influenced the concentrations of FA and AA via their gas−aqueous partitioning, gross production yields, and radical-induced decarboxylation reactions. The data are adequately reproduced with a kinetic model; however, different reaction mechanisms are needed for the low and high pH chemistries. Fewer stable reaction intermediates were observed for 2-MT compared to E and at high pH compared to low pH, providing insight into the decomposition pathways of 2-MT. On the basis of the substantial production yields and partitioning of FA and AA in the aqueous photooxidation of 2-methyltetrol, aqueous aging of isoprene-derived SOA may contribute to FA and AA emissions to the atmosphere that are currently missing from models.

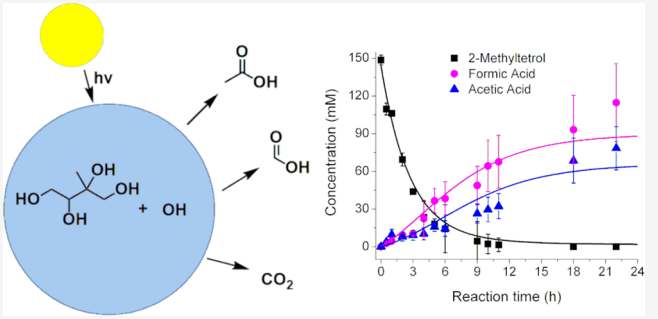

KEYWORDS: *formic acid, acetic acid, isoprene SOA, 2-methyltetrol, aqueous oxidation, atmospheric chemistry, aerosol aging*

INTRODUCTION

Formic acid (HCOOH) and acetic acid (CH_3COOH) are the most abundant gas-phase organic acids in the atmosphere. These small organic acids exert considerable control over atmospheric chemistry and climate by altering aerosol acidity, cloudwater acidity, and cloud condensation nuclei activity of aerosols.[1−4] However, their global sources are not well-understood. Recent satellite observations, surface exchange flux measurements, and modeling consistently show a "missing" source of these acids, particularly over regions of heavy biogenic influence.[5−12] The known gas-phase chemistry of dominant biogenic volatile organic compounds (VOCs), such as isoprene,[13] cannot explain the higher than expected fluxes of formic and acetic acids. Several explanations for the discrepancy between measurements and models have been suggested, including an unconstrained soil source,[10] a direct biogenic source that exceeds prior expectations,[5,9,10] and as yet unknown secondary chemistry.[9,14,15] This work explores a secondary source from the aqueous oxidation of a key secondary organic aerosol (SOA) constituent from the ubiquitous and abundant non-methane hydrocarbon isoprene (C_5H_8).

A particularly important SOA constituent from isoprene is formed from the ring opening of the C_5 epoxydiols (IEPOX),[15] which are the predominant products[16] of the low-NO photooxidation of isoprene in the gas phase. Hydrolysis of IEPOX produces diastereomeric 2-methyltetrol.[17−19] High mass loadings of 2-methyltetrol have been observed globally in aerosol particles, including the Amazon (up to 65 ng/m^3),[20] European boreal forests (up to 33 ng/m^3),[21] Beijing, China (14−17 ng/m^3),[22] the Midwest United States (up to 75 ng/

Special Issue: Mario Molina Memorial

Received: April 15, 2021
Revised: May 18, 2021
Accepted: May 19, 2021

m^3),[23] and the Southeastern United States (up to 216 ng/m^3).[24−26] 2-Methyltetrol can be observed as the single most abundant regional SOA constituent from measurements and modeling.[27−29] Two recent global modeling studies suggest that this IEPOX hydrolysis pathway accounts for 33−37% of all SOA from isoprene or up to 45−48 Tg/year of 2-methyltetrol (20−21 Tg of C/year) produced worldwide.[30,31] These studies also showed that current SOA formation mechanisms tend to overestimate isoprene-derived SOA, which has been suggested is due to an underestimate of chemical losses of SOA constituents, such as condensed-phase oxidation of 2-methyltetrol or other SOA compounds.[32]

2-Methyltetrol in atmospheric aerosol particles will undergo aqueous oxidation in the aerosol liquid water or in the substantially larger volume of liquid water when the aerosols grow to fog and cloud droplets. Taking the liquid water content to be 5 $\mu g/m^3$ in ambient aerosols,[33] 0.01 g/m^3 in fog/haze,[34] and 0.2 g/m^3 in cloud droplets,[35] upper limit concentrations of 2-methyltetrol in atmospheric water in the Southeast U.S. can be roughly estimated to be 7 μM in a cloud droplet, 0.1 mM in a fog droplet, and up to 300 mM in a hydrated aerosol particle (assuming no particle phase separations and based on an loading of ∼200 ng/m^3).[24−26] With OH concentrations estimated in the range from 10^{-14} to 10^{-12} M in these atmospheric aqueous systems,[36] there is substantial chemistry (e.g., rates on the order of 0.01−100 μM/s) that can occur to form small organic acids as well as other products.

However, the true yields of formic and acetic acids from the aqueous oxidation of 2-methyltetrol (or a proxy polyol) remain elusive in the literature.[13] The oxidation of polyols in both the bulk aqueous phase and on sub-micrometer aerosols has been studied previously;[37] however, organic acid yields were not measured. Aqueous-phase oxidation, in particular, has received considerable attention in recent years.[38−43] Such bulk-phase studies have demonstrated that aqueous-phase oxidation, when it occurs, can lead to the rapid formation of highly oxidized organic species,[44−47] among other reactions. Presumably, fragmentation chemistry[48] also occurs, of which the extent has not been quantified but may be highly relevant to formic and acetic acid yields that have not been accounted for in atmospheric models.

Here, we report our bulk-phase investigations into the aqueous hydroxyl radical photooxidation of 2-methyltetrol of isoprene at different pH as a potential source of formic and acetic acids, and compare its chemistry to erythritol, the non-methylated chemical analogue, to gain insights into the chemical mechanism of oxidation. Bulk chemistry of polyols is more relevant to large-curvature droplets compared to sub-micrometer aerosols. It is highly challenging to conduct quantitative yield experiments of 2-methyltetrol oxidation on suspended aerosols given the substantial gas/water partitioning under different environmental conditions. Care should be taken to extrapolate results outside the conditions of the experiments. Results on the oxidation of less volatile polyols and related compounds in the liquid water of suspended sub-micrometer aerosol particles are forthcoming from our group.

METHODS

Erythritol was purchased from Fisher Scientific. D_2O (99.8 atom % D), $CDCl_3$ (99.8 atom % D), acetonitrile (MeCN, ≥99%), cyclohexane (≥99%), 2,4-dinitrophenyl hydrazine (DNPH, 97%) and 50 wt % hydrogen peroxide (H_2O_2) in water were obtained from Sigma-Aldrich. DNPH was recrystallized prior to use. All other purchased chemicals were used without further purification. Ultrapure H_2O was obtained from a Milli-Q purification system (18 MΩ, Millipore Sigma). 2-Methyltetrol standards were synthesized according to the literature,[49] via the hydrolysis of δ-IEPOX, and confirmed by ^{1}H nuclear magnetic resonance (NMR) at an estimated purity of >95%. Photochemical reactions were performed in a photochemical enclosure equipped with an ultraviolet B (UV-B) broadband fluorescent light with peak wavelength emissions at 310 nm (emission photon flux shown in Figure S1 of the Supporting Information), using H_2O_2 as the OH source. Experiments were performed at a pH range of 2−9 for 2-methyltetrol and at pH ∼ 4 for erythritol (unadjusted). The majority of the data presented are at pH 2−4, where the organic acids were observed with NMR spectroscopy as the neutral species. Across the pH range of 2−4, no differences in yields were observed, within uncertainty, in the same chemical system. Both high-performance liquid chromatography−high-resolution mass spectrometry (HPLC−HRMS) and NMR were used to quantify the parent polyol and select stable reaction products. Overlapping quantifications of polyols by HPLC−HRMS and NMR were performed to ascertain consistency of the data. Results from both methods showed excellent agreement (Figure S2 of the Supporting Information) below 2 h of reaction time for erythritol + OH. Small signals of other polyols arose during the reaction at longer time scales in the NMR analysis; thus, data from HPLC−HRMS were used for yields from erythritol. The 2-methyltetrol reaction had few interferences throughout the reaction period.

HPLC−HRMS was used to analyze polyol concentrations and stable reaction products that have a carbonyl moiety. The carbonyls were converted to hydrazone adducts with 2,4-dinitrophenylhydrazine (DNPH) using a procedure adapted from Zweiner et al.[50] This reaction will also derivatize organic acids but with a much lower efficiency; thus, HPLC−HRMS was not used for organic acid quantification in this work. Derivatization was performed by adding 200 mg of recrystallized DNPH to a 15 mL solution containing HCl (∼12 M, Merck), ultrapure water, and MeCN in the ratio of 2:5:1 (v/v/v). A total of 200 μL of the reaction solution was then mixed with 1 mL of the DNPH solution at room temperature. For the product analysis by HPLC−HRMS, 1 mM polyol was mixed with 10 mM H_2O_2 in a 3.5 mL capped quartz cuvette. The solutions were exposed to the UV lamp for the desired reaction durations, and aliquots were removed every 15 min for 2 h and reacted with the DNPH solution overnight.

HPLC−HRMS used an Agilent 1100 HPLC coupled to a linear trap quadrupole (LTQ) Orbitrap mass spectrometer (Thermo Corp., Waltham, MA, U.S.A.) operating at a mass resolving power of 60 000 $m/\Delta m$ at m/z 400. Separation of polyols was performed isocratically on a Shodex Asahipak NH2P-40 2D column (2 × 150 mm, 4 μm, 100 Å) at a flow rate of 0.3 mL/min, column temperature of 40 °C, and eluent mixture of 90:10 MeCN and water with 0.05% ammonium formate. Separation of DNPH adducts was performed with an Agilent Poroshell EC-C18 column (2.1 × 100 mm, 2.7 μm, 120 Å) using a gradient elution method previously reported elsewhere.[51]

NMR analyses (^{1}H and ^{13}C) were used to quantify formic acid, acetic acid, glycolic acid, and the parent polyol. NMR was also used to qualitatively identify functional groups of stable reaction intermediates. As a result of the lower sensitivity of

https://doi.org/10.1021/acsearthspacechem.1c00107
ACS Earth Space Chem. XXXX, XXX, XXX−XXX

NMR analysis, 75−150 mM polyol was mixed with 1−1.5 M H_2O_2 to increase the analytical signal. Reactions for NMR analyses were performed by directly irradiating the sample within a 5 mm quartz NMR tube rated for 500 MHz. ^1H and ^{13}C NMR data were collected on a 400 MHz Bruker instrument (400 MHz Bruker Avance III HD Nanobay spectrometer) using an autosampler and analyzed using TOPSPIN. Water suppression was run using the standard WATERSUP parameters.

Cyclohexane was used as an internal standard for two NMR experiment setups: (A) the cyclohexane internal standard in $CDCl_3$ was loaded into a glass capillary, flame-sealed, and dropped into a NMR tube containing the reaction mixture, and (B) cyclohexane in $CDCl_3$ was introduced into the NMR tube, and instead, the reaction mixture was loaded into the glass capillary and flame-sealed. The experimental setup in B probes the reaction when little to no headspace is available (in the sealed capillary) for gas/aqueous partitioning of formic and acetic acids, which enables quantification of the total yield for the volatile acids. The setup in A captures only the aqueous concentration of acids. B undergoes a slower reaction through the glass capillary compared to the quartz exterior of the NMR tube (60% lower steady-state concentration of the OH radical). Thus, all reactions have been normalized to their OH exposure (steady state [OH] × reaction time) for this set of experiments.

RESULTS AND DISCUSSION

Reaction Kinetics and Yields of Small Acids. The decay kinetics of erythritol (E) and 2-methyltetrol (2-MT) as well as formation of product compounds were monitored via ^1H and ^{13}C NMR. ^1H NMR shows the proton environment on every molecule that is present in the solution, although protons on OH groups are often weak or missing as a result of their rapid exchange with D_2O. As such, multiple signals are observed and remain unidentified, especially as these peaks overlap with other signals. In both the erythritol (E + OH) reaction (Figure 1) and 2-methytetrol (2-MT + OH) reaction (Figure 2),

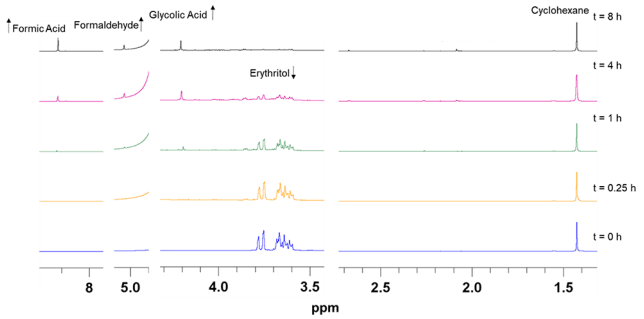

Figure 1. ^1H NMR spectra at five different time points for the erythritol + OH reaction.

several peaks are distinct and easily identifiable based on previously reported data for C_1−C_3 oxidation products;[52−54] these include formic acid, acetic acid, and glycolic acid, and the signals for hydrated formaldehyde dimer, as shown in Table S1 of the Supporting Information. Formic acid is easily quantifiable without interference at 8.2 ppm. Acetic and glycolic acids are also quantifiable, but with slightly higher uncertainty as their peaks overlap with contributions from other minor, structurally similar, species. Formaldehyde is

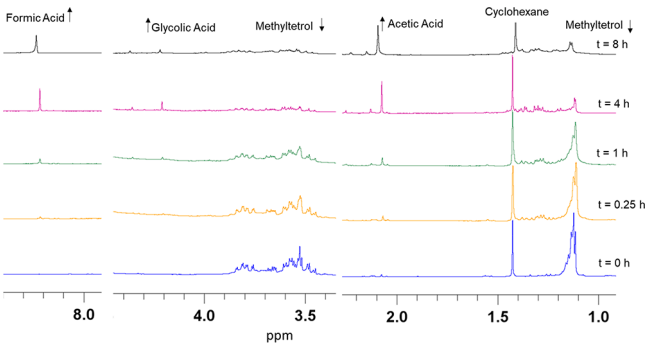

Figure 2. ^1H NMR spectra at five different time points for the 2-methyltetrol + OH reaction. Note that, at 8 h, the peak of cyclohexane shifted with respect to the acids.

hydrated and, thus, is significantly harder to accurately quantify as the peak strongly overlaps with the tail of the residual water signal, making an accurate peak area analysis difficult.

The steady-state OH concentrations used in the experiments are relevant to the atmospheric aqueous phase at approximately (8−10) × 10^{-14} M, estimated using the second-order OH kinetic coefficients of erythritol (1.9 × 10^9 M^{-1} s^{-1})[36] and 2-methyltetrol (1.1 × 10^9 M^{-1} s^{-1}).[55] Figure 3 shows the OH oxidation experiment of 2-methyltetrol at solution pH 2, where the precursor is reacted away and small acids are formed over the course of ∼24 h.

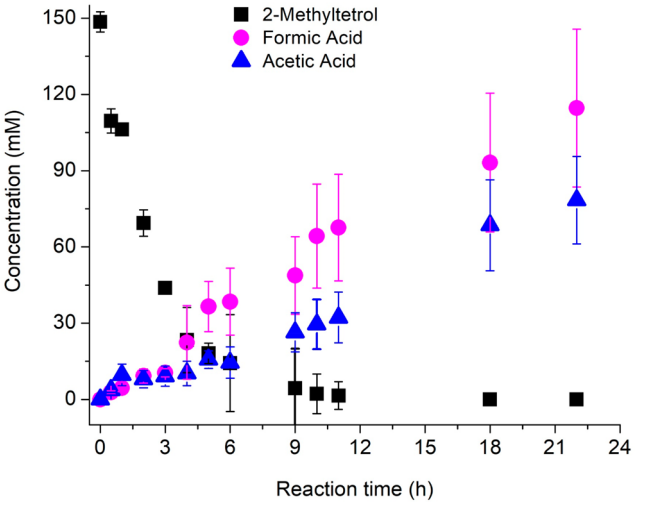

Figure 3. Absolute concentrations of precursor 2-methyltetrol and product acids during the course of OH oxidation, as quantified by ^1H NMR. Error bars represent 1 − σ deviations from repeated experiments.

The absolute molar yields, defined as 100% × (moles of product formed)/(moles of reacted polyol), of formic acid (FA, ∼78%) and acetic acid (AA, ∼53%) at 18 h exceed the moles of 2-methyltetrol reacted because the precursor has 5 carbons and the products have 1−2 carbons. Thus, we define the per carbon molar yield as

$$\text{percent molar yield per carbon} = 100\% \times \left(\frac{\text{mole product formed}}{\text{mole reactant lost}}\right) \times \left(\frac{\#C_{\text{product}}}{\#C_{\text{reactant}}}\right)$$

https://doi.org/10.1021/acsearthspacechem.1c00107
ACS Earth Space Chem. XXXX, XXX, XXX−XXX

The molar yield per carbon defined above has a maximum of 100%. Thus, the molar yields of FA and AA translate to ~15 and ~21% at 18 h, respectively. The yields of these product acids are not constant because the further oxidation of C_2-C_5 stable intermediate products will produce FA and AA, even when the precursor is all reacted away. In addition, the further oxidation of FA and AA or their dissociated forms in solution will affect yields. Gross production yields are discussed in the Kinetic Modeling section.

The per carbon yields of products in the E + OH and 2-MT + OH reactions (Figure 4) show that the evolution of small

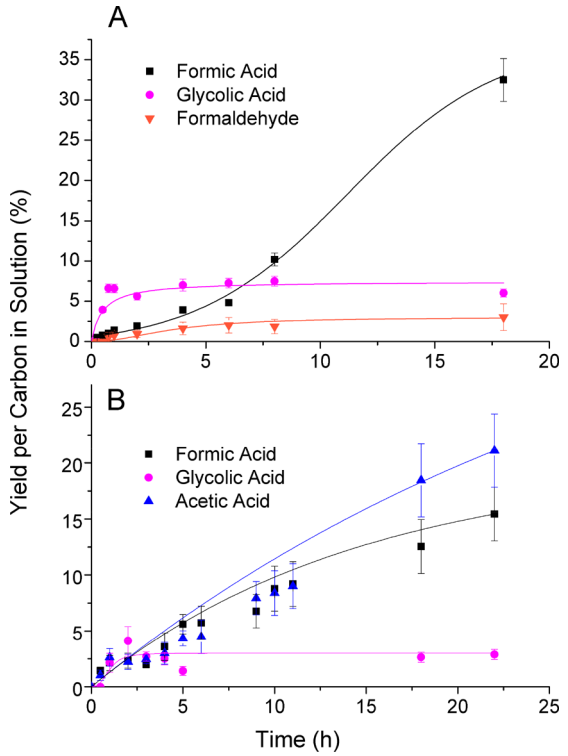

Figure 4. Molar yields per carbon of the oxidation products of (A) erythritol and (B) 2-methyltetrol.

acids is different between the two experiments. Glycolic acid (GA, $C_2H_4O_3$) is an important stable intermediate species in both reactions. GA appears as a first-generation product and is both produced and reacted away quickly over the course of the experiments. In the E + OH reaction (Figure 4A), GA is formed first and FA does not reach the yields of GA until several hours later. AA is not expected as a product in the E + OH reaction because erythritol does not have a methyl group. In the 2-MT + OH reaction (Figure 4B), FA and AA form simultaneously with GA and continually rise over the duration of the reaction.

In addition, FA and AA together in solution can only account for ~35% of carbon of 2-MT after all 2-MT is reacted away at 22 h of reaction. Some of the "missing" yields that are not observed as FA, AA, and other products shown in Figure 4 can be reconciled as CO_2. Figure 5 (blue) shows that the only peaks observed in the ^{13}C NMR spectra from the 2-MT + OH reaction at time zero belong to 2-MT, $CDCl_3$, and the cyclohexane internal standard, as expected. After 18 h of photooxidation (Figure 5, magenta), peaks at 176 and 20 ppm are observed, which correspond to AA, and a peak at 165 ppm is observed, which corresponds to FA. The only other product

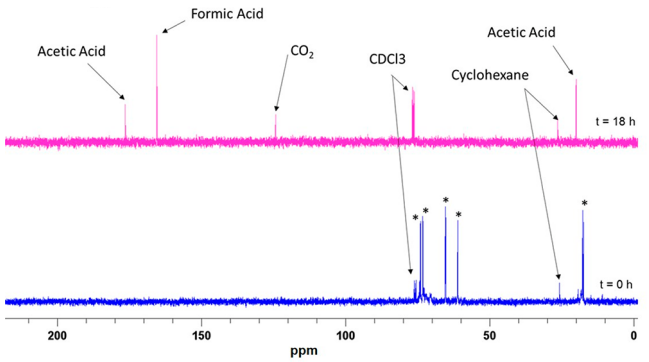

Figure 5. ^{13}C NMR of the 2-methyltetrol + OH reaction at 0 and 18 h reaction time. Asterisks denote peaks that belong to the 2-methyltetrol reactant.

peak observed is at 124 ppm, which corresponds to CO_2. The yield of CO_2 is somewhat uncertain, and integrations between the two acetic acid peaks is not 1:1, as expected, which highlights the difficulty in using this method for quantification. However, given that the integrations between the formic acid, cyclohexane, and CH_3 peak give a very similar ratio to those observed in ^1H NMR, observed CO_2 can be estimated to account for another ~10−15% of the carbon yield as a lower limit. This minimum estimate does not account for the partitioning of CO_2 into the gas phase.

Effect of Volatile Partitioning. A portion of the carbon yield that is not observed as FA, AA, or CO_2 in solution will have partitioned to the gas phase via effective Henry's law partitioning, a process that is pH-dependent for all three products. We attempted to quantify the total balance of mass by limiting the partitioning process in the little to no headspace experiment, wherein the reaction is run in a sealed capillary instead of an open NMR tube. Figure 6 shows that limiting the headspace partitioning for FA, AA, and GA consistently

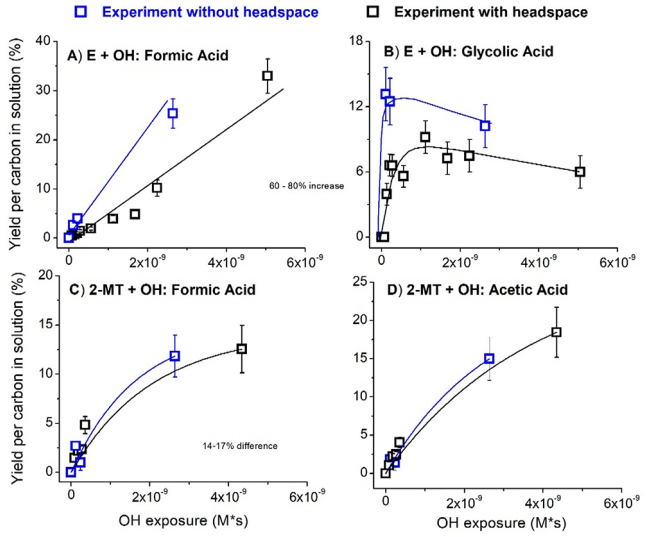

Figure 6. Carbon yields for select products in the erythritol (E) + OH experiment and 2-methyltetrol (2-MT) + OH experiment when performed in an open NMR tube and inside a sealed capillary to remove headspace to limit the partitioning of volatiles. The sealed capillary does not remove 100% of the headspace, and one experiment may have more headspace than another. Solid lines are included to guide the eye.

https://doi.org/10.1021/acsearthspacechem.1c00107
ACS Earth Space Chem. XXXX, XXX, XXX−XXX

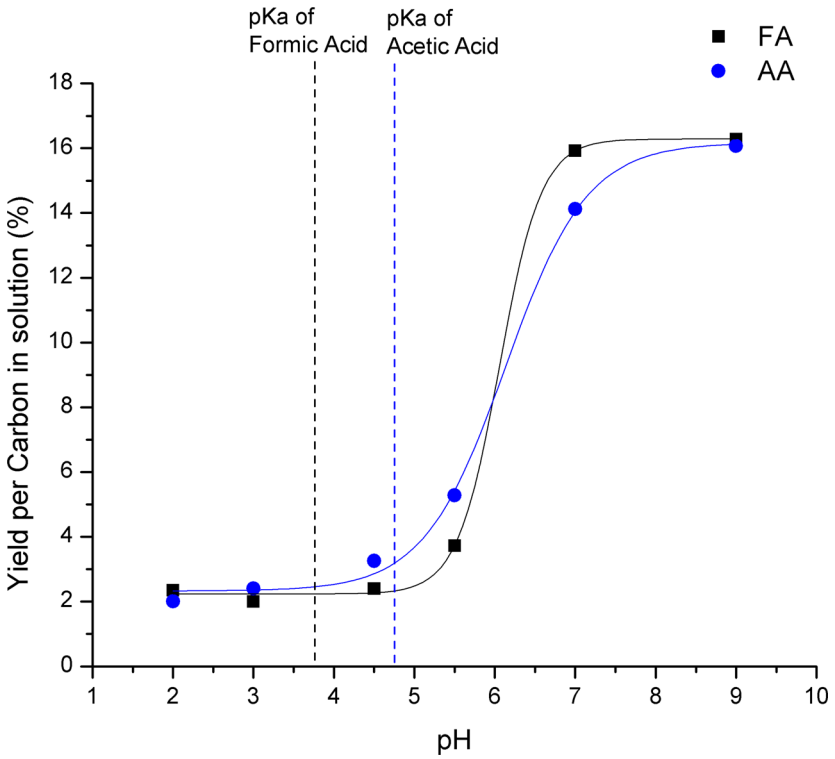

Figure 7. Effect of solution pH on the observed yields of formic and acetic acids in solution from the 2-methyltetrol + OH experiment after 30 min of reaction time. At basic pH, the organic acids were observed as their carboxylates. pH was measured directly after the ^{1}H NMR spectrum was obtained. Lines shown are Boltzmann fits of the data.

enhances the carbon yield. The yield enhancement is 15−18% in the 2-MT + OH experiment and 60−80% in the E + OH experiment. The discrepancy between the E and 2-MT experiments is not due to the reaction itself but likely due to the challenges of obtaining consistent results in the sealed capillary experiments. The E + OH reaction sample had less headspace than the 2-MT + OH sample. The heat-sealing process was performed by hand; it is highly challenging to remove all headspace or standardize the amount of headspace in different capillaries. We do not believe that the different results are due to pH. The 2-MT capillary experiment (pH ∼ 2) was slightly more acidic than the E + OH experiment (pH ∼ 4); however, the yields of FA and AA from the 2-MT oxidation at any given time point did not change in the range of pH 2−4 (Figure 7). Multiple attempts were needed to balance the internal standard concentrations (in the outer NMR tube) with the reaction signals, which limited our ability to obtain data from every capillary that was generated. In addition, we were not able to estimate the enhancement in CO_2 yields in the absence of partitioning given the much lower sensitivity of the ^{13}C technique. We believe the E + OH experiment (panels A and B of Figure 6) produced a more reliable result; however, we constrain the total product yields to upper bounds (yield in solution + 80%) and lower bounds (yield in solution + 15%) as supported by the entirety of the data. CO_2 was assumed to act similarly to small acids in terms of Henry's partitioning, an assumption that may not be correct.

Table 1 shows that FA, AA, and CO_2 can be estimated to account for approximately 60−100% of carbon from 2-MT oxidation when extrapolated to a reaction time of infinity using a rise to maximum exponential fit for FA and AA and when using data taken at 18 h for CO_2. The upper limit estimate offers a rough carbon closure for the reaction, although we expect CO, formaldehyde, and possibly other compounds to also be products of the reactions at longer time scales. Even with the uncertainty in obtaining total carbon closures, it is clear from the data that the three products shown in Table 1 account for the majority (∼ 60%), if not the entirety, of molar carbon lost from 2-MT when oxidized with OH.

Table 1. Carbon Yields of Products in the 2-Methyltetrol + OH Reaction

2-MT + OH reaction	% yield (C) in solution	% yield (C) in solution and gas	
oxidation product	extrapolated to $t = \infty$	lower limit estimate	upper limit estimate
formic acid	15	17	27
acetic acid	24	28	43
carbon dioxide	10−15 (at 18 h)	12	27
total	49−54	56	97

Effect of Solution pH for 2-Methyltetrol + OH. Solution pH was adjusted at time zero using small amounts of aqueous NaOH because the unadjusted 2-MT solution derived from using the synthesized standard is at pH 2. Solution pH decreases over the course of a 24 h experiment as a result of the production of the organic acids from the parent polyol. NMR is able to differentiate between the neutral (HA) and deprotonated (A^-) forms of the carboxylic acids based on their chemical shifts, lending insight into the acid dissociation equilibria during the experiment. The chemical shifts[56] are 8.2 ppm for FA and 2.2 ppm for AA at pH 2. This transitions to 8.4 ppm for formate and 1.9 ppm for acetate above pH 5. We opted to not use buffer solutions to alleviate this pH shift because this would introduce potentially reactive species into

https://doi.org/10.1021/acsearthspacechem.1c00107
ACS Earth Space Chem. XXXX, XXX, XXX−XXX

the system and may alter the decay and production of observed species.

Because the solution pH decreases during the course of the experiments as a result of the conversion of polyol to organic acids, we performed experiments at a fixed reaction time (30 min) and determined the pH with a calibrated electrochemical probe directly after the NMR yield measurements for formic/formate and acetic/acetate. The effect of solution pH on the solution-phase yields of FA and AA (or their carboxylates) is a complex interplay between gas−aqueous partitioning and alterations of the oxidation chemistry. Figure 7 shows that the aqueous carbon yields observed for the relevant products at the 30 min mark highly depend upon pH. The solution pH determines whether FA, AA, or their carboxylate forms exist in solution. The observed behavior is consistent with the fact that the anions are not volatile, and thus, all of their yield would be observed in solution compared to the acids. The pK_a values of the acids are denoted on the figure, which do not match the inflection point of the yield graph. However, this may be expected because standard pK_a values are generally measured in pure water and pK_a values will increase in solution when other organic constituents are present.[57]

However, the observed relationship shown in Figure 7 cannot be explained entirely by partitioning. The headspace experiments suggests that up to perhaps a 2-fold increase in yield throughout the experiment can be expected when gas−aqueous partitioning is suppressed, whereas the yield increase as a result of pH (between the acid and carboxylate species) is, remarkably, a factor of 8 different. Thus, at basic pH, FA/AA (that dissociate into formate/acetate) are likely formed at much higher yields in the reaction at the 30 min mark compared to the same reaction at acidic pH. This is corroborated by modeling (see the Kinetic Modeling section). We rule out slower loss processes for carboxylates because those anions actually have a faster reaction rate coefficient with OH (chemical loss) compared to their protonated counterparts and do not partition to the gas phase (physical loss).[58]

Figure 8 shows that, at low levels of OH exposure, a drastic increase in the yields of formate/acetate (C and D) present in solution is observed in comparison to their conjugate acids (A and B), which is consistent with the data in Figure 7 for the reaction at the 30 min mark. However, after the initial rise in yields that may be dominated by formation pathways from 2-MT, formate begins a sharp decrease until it has all been consumed entirely. Acetate also sees a decrease but at a significantly slower trend. The reactions responsible for the loss of formate and acetate at higher OH exposure are likely decarboxylations induced by radical chemistry. We rule out thermal decarboxylations because the temperatures required (e.g., >300 °C)[59] are much higher than the present experiments. The reaction of OH + $HCOO^-$ → H_2O + CO_2^- is fast ($k \sim 3.4 \times 10^9$ M^{-1} s^{-1}) compared to the OH + HCOOH reaction ($k \sim 1 \times 10^8$ M^{-1} s^{-1}). The OH + CH_3COO^- reaction ($k \sim 7 \times 10^7$ M^{-1} s^{-1}) is also faster than the OH + CH_3COOH reaction ($k \sim 1 \times 10^7$ M^{-1} s^{-1}) but much slower than the same reaction for formate.[58] All of these reactions will eventually produce CO_2 in aqueous solution. The rate constants are consistent with the yield relationships of formic acid, acetic acid, formate, and acetate in Figure 8 and further suggest that the lower formic acid yield (~15% C at long OH exposures) compared to acetic acid (~22% C at long OH exposures) at pH < 5 in the 2-MT + OH reaction is not entirely due to a lower formation rate of FA compared to AA but, in addition, a faster loss rate of FA + OH compared to AA + OH.

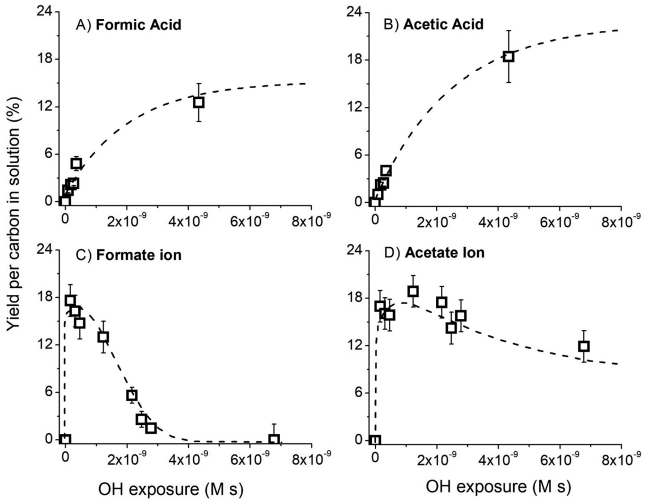

Figure 8. Aqueous carbon yields of formic and acetic acids (experiments at pH 2) and their carboxylates (experiments at pH 9) from the 2-methyltetrol + OH reaction as a function of the OH exposure time. The concentrations observed in solution represent the ratio of sources and sinks of these acids/carboxylates. The dashed lines are to guide the eye.

Identification of Stable Intermediate Species. Eventually all polyol carbons will be converted to FA, AA, and CO_2 (and possibly also CO and formaldehyde); however, smaller signals of stable reaction intermediates can be observed at earlier times in the reaction that may help elucidate chemical mechanisms. These signals of reaction intermediates are observed by magnifying the ^1H and ^{13}C NMR spectra to highlight various functional groups as well as via trapping any carbonyl product as hydrazones to be analyzed in HPLC−HRMS. A notable difference between E + OH and 2-MT + OH appears to be the relative lack of larger reaction products for 2-MT. This observation is consistent across NMR and HPLC−HRMS data, despite a 100-fold difference in precursor concentrations between the two techniques. The difference is also consistent across the pH range of 2−4.

Magnifications of the ^1H NMR spectra show that the reaction of E + OH at 15 min (Figure 9, blue) produces compounds that have geminal diol protons around 5 ppm (which may be hydrated aldehydes). Correspondingly, low aldehydic proton signals (HCO) between 8 and 10 ppm accompany the diol signals. Other peaks in the 5−6 ppm region may indicate cyclization, hydration, or oligomerization of these aldehydes.[60] Protons that are adjacent to alkyl groups [HC(R)(R′)−OH] can be observed at 3−4 ppm. It is clear that many of these peaks do not belong to the precursor, although it is difficult to disentangle in a mixture of polyols and their products in this region. β-hydroxy carbonyls or acid protons can be attributable to shifts between 4 and 4.8 ppm. Two singlets stand out distinctively at 4.54 and 4.57 ppm, and although the identity of these is unknown, their chemical shift roughly matches those observed for RCOCHOH for tartaric acid.[61] Tartaric acid can be produced by oxidizing the two end $-CH_2OH$ groups in erythritol to −COOH groups. The 2-MT + OH (Figure 9, magenta) reaction produce these similar functional groups but at much lower abundance. Even though the reaction of 2-MT + OH is slower, it forms FA faster than E

https://doi.org/10.1021/acsearthspacechem.1c00107
ACS Earth Space Chem. XXXX, XXX, XXX−XXX

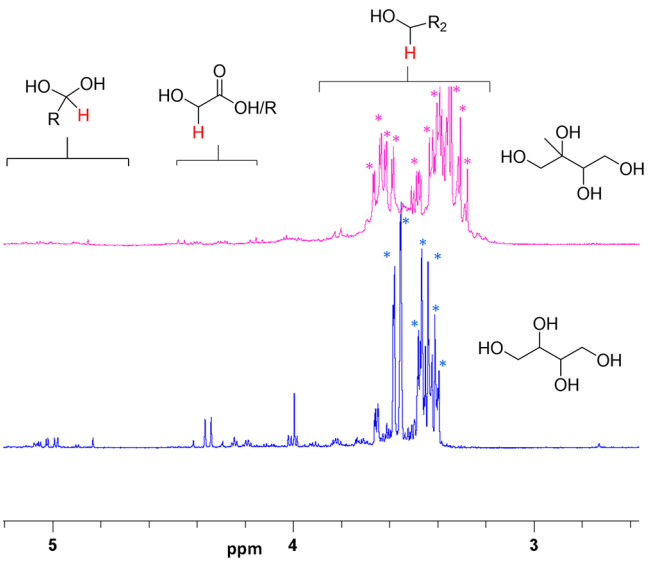

Figure 9. Magnification of the 3−6 ppm region in the ^{1}H NMR spectra for 2-MT + OH (magenta) and E + OH (blue) experiments after 15 min of reaction time, performed with water suppression and t = 0 subtraction, showing stable intermediate products. Asterisks denote hydrogens belonging to the parent polyols.

+ OH, which suggests that instead of forming the larger stable intermediate compounds, 2-MT oxidation produces FA, AA, and CO_2 more promptly.

Likewise, ^{13}C NMR (Figure 10) shows a multitude of stable intermediates in the reaction of E + OH (blue) and a relative

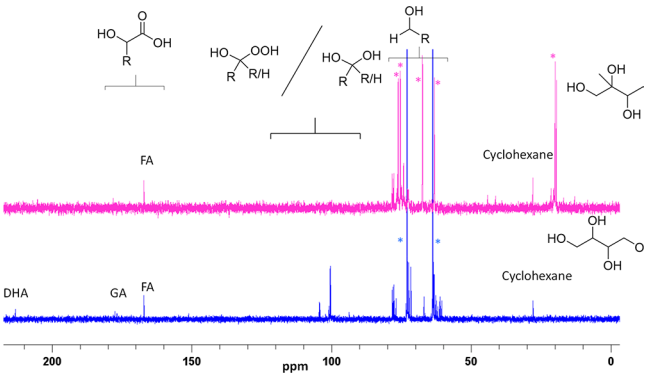

Figure 10. ^{13}C NMR spectra for 2-MT + OH (magenta) and E + OH (blue) experiments after 30 min of reaction time. Asterisks denote carbons belonging to the parent polyols.

lack of stable intermediates in the 2-MT + OH reaction (magenta). Note that erythritol only has two types of carbons as a result of symmetry, whereas 2-methyltetrol has five distinct carbon environments; thus, the signal integration for 2-MT is more spread out across the different carbons, but their initial concentration is the same. Figure 10 shows the two reaction mixtures of E + OH and 2-MT + OH on the same scale as normalized by the cyclohexane internal standard. From these spectra, we can ascertain the identity of a few additional species, of which some were not previously identifiable from the ^{1}H NMR. In the E + OH reaction, the peak at 211 pm corresponds to C═O of ketones and coupled with the CH_2 peak at 65 ppm highlights the presence of dihydroxyacetone. At 175 ppm, there are at least two peaks. Within this region, we observe carboxylic acid groups; thus, these are likely glycolic acid and some structurally related C_3 or C_4 carboxylic acid species. In the C−OH region between 55 and 80 ppm, next to CH (71 ppm) and CH_2 (62 ppm) of erythritol, there exist at least 9 CH and 12 CH_2 peaks corresponding to a multitude of intermediate species, of which all contain CH−OH.

An expansion of the 60−100 ppm region that is present in Figure 10 is shown in Figure S3 of the Supporting Information, highlighting the most interesting peaks around 90−105 ppm that each contain a $C(OH)_2$ or C(OH)(OOH) group. The most upfield peak at 92 ppm corresponds to the hydrolyzed formaldehyde dimer. The identities of the remaining peaks are uncertain, but it is clear that the peaks around 99−100 ppm are CH groups and are also likely generated from the hydration of C_3−C_4 aldehydes. The two peaks around 102 ppm are quaternary carbons but are more downfield than potential hydrated ketone (which will be less favored than hydrated aldehydes). The hydrated dihydroxyacetone peak occurs at 95 ppm, and hydrated mesoxalic acid occurs around 96 ppm. Thus, an alternative assignment for these peaks at ∼100 ppm is a carbon attached to a OH and OOH group because it has been reported that, for $R_3C(OOH)$ compounds, the hydroperoxide signal is between 8 and 12 ppm more downfield than its equivalent alcohol.[62] Few ^{13}C NMR spectra for C(OH)(OOH) compounds have been reported; one study on the photooxidation of pyruvate observed a signal at 102 ppm for hydroperoxide.[63] Hydroxy-hydroperoxides are well-known intermediates in OH-initiated reactions of hydrocarbons in the presence of oxygen;[64] therefore, these assignments are consistent with our expectations of the OH chemistry if parallels can be drawn to the gas phase. Hydroxy-hydroperoxide moieties are also assigned to some highly oxidized intermediates observed in the HPLC−HRMS spectra. Thus, we conclude that there are at least two stable compounds in solution that possess $(OH)CR_2(OOH)$ groups at 102.4 and 102.7 ppm. However, we cannot rule out the potential for the existence of (OH)CHR(OOH) groups for some or all of the four peaks at 98−99 ppm. The same reaction setup with 2-MT did not gain any further mechanistic insight because no other peaks were observed above the detection limit in the ^{13}C NMR spectra, even after 2.5 h of irradiation.

In agreement with NMR, the HPLC−HRMS data for reactions performed at 1 mM precursor concentrations also show that the 2-MT + OH reaction does not abundantly form the larger stable intermediates in the reaction chain on the way to smaller volatile products. Figure 11A shows that the E + OH reaction abundantly produces a C_4 first-generation trihydroxy carbonyl (observed at m/z 299.06 as its DNPH adduct); this signal is the largest signal observed in HPLC−HRMS for the reaction at shorter time scales. In comparison, the 2-MT + OH reaction produces the equivalent C_5 first-generation trihydroxy carbonyl (Figure 11B, observed at m/z 313.08 as its DNPH adduct) at roughly one-tenth of the yield of the analogue in the E + OH reaction. Although only one isomer structure is shown in Figure 11 for simplicity, two isomers of the erythritol C_4 trihydroxycarbonyl can be observed to be peak-resolved but not baseline-resolved. The larger chromatographic peak in Figure 11A can be assigned to the ketone produced from the OH abstraction at the secondary carbon as opposed to the aldehyde produced from the OH abstraction at the primary carbon. The relative abundances are as expected on the basis of the thermodynamic favorability of the resulting alkyl radicals.[65] All reaction products observed as DNPH adducts in HPLC−

https://doi.org/10.1021/acsearthspacechem.1c00107
ACS Earth Space Chem. XXXX, XXX, XXX−XXX

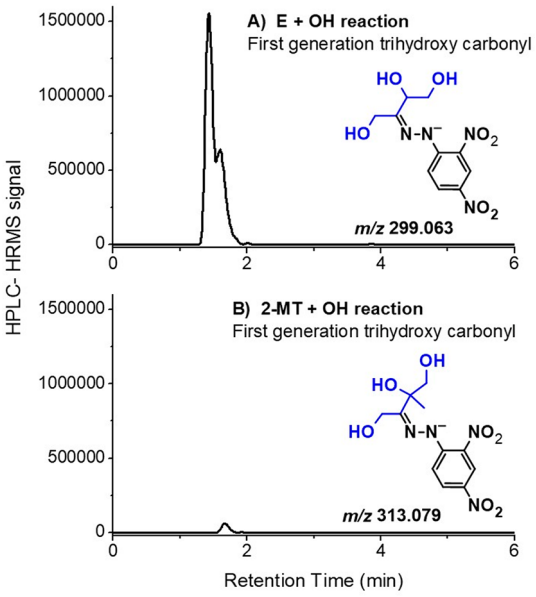

Figure 11. HPLC−HRMS single ion chromatograms showing the abundance of the first-generation carbonyl products (observed as DNPH adducts) of the (A) erythritol + OH reaction and (B) 2-methyltetrol + OH reaction at roughly the 60 min mark.

HRMS are listed in Table S2 of the Supporting Information (E + OH) and Table S3 of the Supporting Information (2-MT + OH).

Reaction Mechanism. It is well-understood that OH will abstract hydrogen from molecules with a saturated CH bond, including polyols. For erythritol and 2-methyltetrol, this process will mainly produce α-hydroxyalkyl (R) radicals in the secondary position (Scheme 1), at approximately a 4:1 preference over the primary position and with negligible abstraction of the OH hydrogen.[66] Most of the aqueous oxidation of polyols has been studied in the presence of metal catalysts as a result of the industrial applications of this reaction.[67,68] Very limited information is available in the literature regarding the fates of the α-hydroxyalkyl radicals in the chemical regime most relevant to atmospheric aqueous phases. In the gas phase, α-hydroxyalkyl radicals readily lose HO_2 (from reaction with O_2) to form the carbonyl.[69] It is not clear if HO_2 loss from the alkyl radical will occur in the aqueous phase given the high intermolecular interactions in solution. As a result of a lack of information on this reaction in the aqueous literature, we do not discuss it further, although we cannot rule out the reaction based on our data. In concentrated aqueous solutions, α-hydroxyalkyl radicals may dimerize to a vicinal diol or disproportionate to an alcohol and

Scheme 1. Proposed Reaction Mechanism of OH + (A) Erythritol and (B) 2-Methyltetrol, Showing the Dominant H Abstraction Pathway from the Secondary Carbon[a]

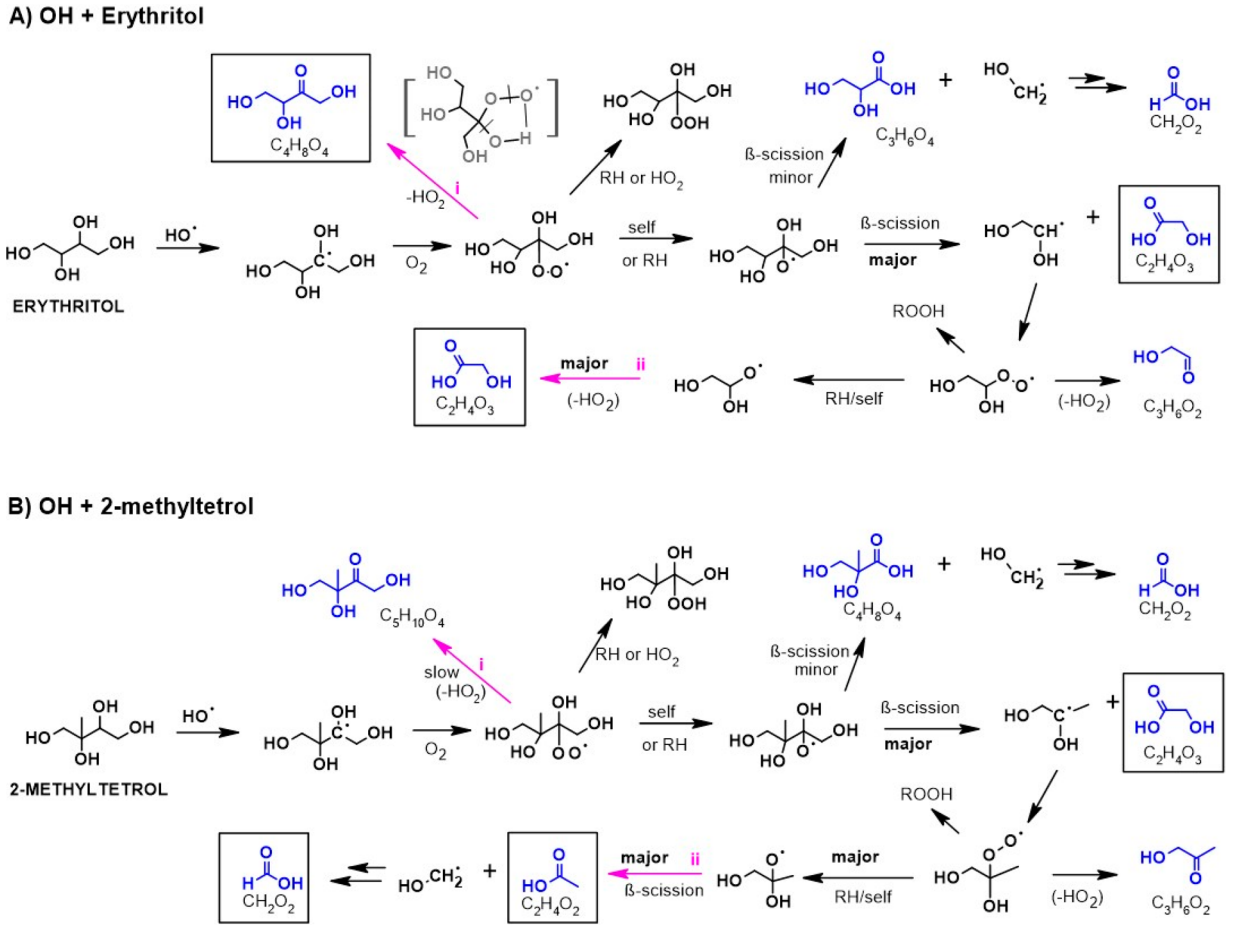

[a]Select first-generation oxidation products, as observed by NMR and HPLC−HRMS, are shown in blue. The volatile organic acids that are the focus of discussion in the text are shown in boxes.

https://doi.org/10.1021/acsearthspacechem.1c00107
ACS Earth Space Chem. XXXX, XXX, XXX−XXX

a carbonyl.[70] They may further reduce organics by transferring hydrogen, becoming a carbonyl.[71,72]

The addition of O_2 to R to form the α-hydroxyperoxy (RO_2) radical has been documented in aqueous solution.[73] On the basis of our observations of α-hydroxyhydroperoxides (ROOH; Figure 8), we suggest that RO_2 chemistry has a prominent role in the aqueous chemical system studied in this work. The α-hydroxyperoxy radicals may intramolecularly lose HO_2, via a cyclic intermediate,[74] to form the carbonyl in less concentrated aqueous solutions but is always in competition with bimolecular reactions involving other RO_2 or RH that will be important for more concentrated solutions (e.g., on organic compounds dissolved in particle liquid water). For some α-hydroxyperoxy radicals, such as the α-hydroxyperoxy radical formed in the C_1 position of glucose or the $^{\bullet}OOHC(OH)_2$ radical, the rate of HO_2 elimination is unusually fast,[75] which will outcompete bimolecular reactions. The experiments of Bothe and co-workers highlighted various substituent effects α to the RO_2 carbon and the strong influence by the solvent environment.[75] Both the expected $RCOH(OO^{\bullet})CH_2OH$ radicals from erythritol and 2-methyltetrol will be secondary; thus, there should be not much difference in their HO_2 loss rates from substitution effects at the α carbon alone. However, the nature of the R group in the $RCOH\ (OO^{\bullet})CH_2OH$ radicals is different, wherein the R group is a tertiary carbon for 2-methyltetrol and secondary for erythritol. Whether the degree of substitution of carbon β to the hydroxyperoxy group will affect the HO_2 loss from these specific RO_2 is still an open question. Experiments with the many carbon centers of glucose show that the β carbon environment may have significant effects;[76] however, it is not straightforward to extrapolate from a cyclic compound to an aliphatic compound. Scheme 1 shows the proposed reaction mechanism for E + OH and 2-MT + OH. To explain the relatively high yields of the first-generation trihydroxycarbonyl of erythritol ($C_4H_8O_4$; Figure 11A) and the relatively low yields of the same first-generation product from 2-methyltetrol ($C_5H_{10}O_4$; Figure 11B), we hypothesize that the HO_2 elimination from the α-hydroxyperoxy radical of erythritol occurs much faster than the analogous reaction for 2-methyltetrol (pathway i in panels A and B of Scheme 1), such that the α-hydroxyperoxy (RO_2) loss fate for 2-methyltetrol through bimolecular chemistry is highly competitive.

If the α-hydroxyperoxy radical is allowed to react bimolecularly, it can be reduced to a substituted alkoxy radical (RO) by collisions with other RO_2 or RH. In the gas phase, it is understood that RO will lose HO_2 upon collisions with O_2 if α carbon is attached to hydrogen [$RHC(R')-O^{\bullet}$], producing a carbonyl.[77,78] Again, it is not clear if the same reaction can be expected in the aqueous phase, although there likely exist a multitude of ways for the primary hydroxyalkoxy radical to lose H in solution to form the stable organic acid (pathway ii in Scheme 1A). However, the hydroxyalkoxy radical for 2-methyltetrol is not attached to H, so that β-scission is the primary fate of that particular hydroxyalkoxy radical (pathway ii in Scheme 1B), propagating an alkyl radical with an organic acid co-product. The cleavage reaction will favor larger alkyl radical decomposition products,[79] preferentially forming the C_3 hydroxyalkyl radical and glycolic acid (GA) instead of the C_1 alkyl radical and 2-methylglyceric acid. The C_3 hydroxyalkyl radical will form RO_2, and then RO and cleave to AA and FA. We expected the C_3 RO_2 to lose HO_2 to form hydroxyacetone fairly prominently;[80] however, we did not observe high hydroxyacetone signals in the HRMS, and it is not clear why.

Thus, in the E + OH system, the major initial products of the reaction will be GA and the C_4 trihydroxycarbonyl, primarily through the HO_2/H loss pathways. In contrast, for the 2-MT + OH system, the RO cleavage pathway can form GA, FA, and AA in the initial generations. Indeed, Figure 4 shows that GA, FA, and AA form more promptly in the 2-MT + OH reaction and at approximately the same rate in the earlier time scales of the experiment. At longer time scales, the loss reactions of GA dominate over its production. Glycolic acid will oxidize to oxalic acid, CO_2, and formic acid (Scheme S1 of the Supporting Information). Oxalic acid will exist as HCO_4^- in the solutions under study, because the pH range we examined is above 2 and the first pK_a of oxalic acid is 1.2. HCO_4^- will likely form two CO_2 molecules or CO_2 and formate in solution with radiation-produced radicals.[81] The C_4 trihydroxycarbonyl of erythritol will also oxidize to produce FA and other products following the same chemistry shown in Scheme 1. Thus, the yields of FA continue to rise in the E + OH reaction (Figure 4A) as its concentration accumulates from several generations of reaction. Because the 2-MT reaction is hypothesized to form FA and AA in a few generations of oxidation, the yields of FA and AA build quickly but start to level out as their losses compete with formation when 2-MT is all removed from the solution.

Kinetic Modeling. We used a simple kinetic model (Mechanism S1 of the Supporting Information) to fit the reaction data to provide gross production yields that account for the multi-generational production and photochemical loss of FA and AA (or their carboxylates) during the course of the reaction (Figure 12). In addition to measured concentrations,

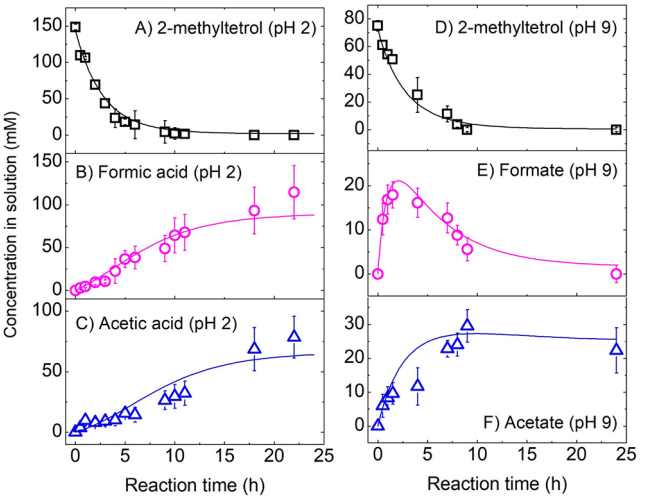

Figure 12. Model fits to concentration data for aqueous photochemistry experiments performed at (A–C) pH 2 and (D–F) pH 9.

the known OH-initiated kinetic coefficients[55,58] of 2-MT, FA, AA, formate, and acetate served as constraints. The model only required 1–2 effective stable intermediates of 2-MT to be considered to satisfactorily reproduce observations. All yields and, in some cases, kinetic coefficients of unknown intermediates are treated as tunable parameters, i.e., degrees of freedom. Thus, these modeling results may represent only one, out of likely multiple, possible solution to this set of coupled differential equations. In addition, the model does not consider gas–aqueous partitioning at pH 2, and a correction

https://doi.org/10.1021/acsearthspacechem.1c00107
ACS Earth Space Chem. XXXX, XXX, XXX–XXX

needs to be applied as in Table 1. Partitioning corrections are not needed at pH 9 because the carboxylates are non-volatile.

Despite caveats, the modeling exercise yielded a number of valuable insights. First, the production of FA and AA from 2-MT in the first generation is much larger at pH 9 (1.3 and 0.45, respectively) than at pH 2 (0.1 and 0.05, respectively), even though the rate of oxidation of 2-MT by OH can be modeled with the same kinetic coefficient. Second, fewer stable intermediate species are required to sufficiently fit the data in the higher pH experiments. This result is well-supported by the NMR data (Figure S4 of the Supporting Information), where the signals of reaction intermediates observable at pH 2 disappear at pH 9.

Although solution pH is not expected nor observed to alter the initial H abstraction by OH in a way that changes the lifetime of 2-MT in solution (panels A and D of Figure 12), pH may severely impact the resulting RO_2 chemistry. For example, solution pH shifts the acid−base equilibrium for the dissolved HO_2 radical (pK_a of 4.8),[82] a bimolecular reaction partner for RO_2 radicals. HO_2 will be the main species in solution at pH 2, while its conjugate base, the superoxide anion radical ($O_2^{\bullet -}$), will be predominantly favored at pH 9. Thus, RO_2 chain termination pathways, such as $RO_2 + HO_2 \rightarrow$ ROOH, to make large stable intermediates will be suppressed at higher pH, allowing other RO_2 fates to dominate, such as reduction of RO_2 to RO. Scheme 1b shows that, once RO is formed from 2-MT, it quickly decomposes to glycolic acid, FA, and AA in high yields. The equilibrium shift of HO_2 alone can explain why only one reaction intermediate and high first-generation yields of FA and AA result from modeling the reaction at pH 9 compared to pH 2, although it may not be the only explanation.

According to Scheme 1b, the singular reaction intermediate at pH 9 will be glycolic acid (pK_a of 3.8), which will be present as glycolate in solution. Glycolate reacts with OH (Scheme S1 of the Supporting Information) to generate FA that then becomes formate. The exceptionally simple chemistry at pH 9 can be modeled by two known reactions while tuning the product yields to best fit the data. Thus, the results are well-constrained.[83]

$$\text{2-MT} + \text{OH} \rightarrow 1.3\text{formate} + 0.45\text{acetate} + 1\text{glycolate} \quad (k_1 = 1.14 \times 10^9\ \text{M}^{-1}\ \text{s}^{-1}) \quad (1)$$

$$\text{glycolate} + \text{OH} \rightarrow 1\text{formate} + 1\text{CO}_2 \quad (k_2 = 8.6 \times 10^8\ \text{M}^{-1}\ \text{s}^{-1}) \quad (2)$$

At pH 2, the mechanism is more complex after the decay of 2-MT (Mechanism S1 of the Supporting Information), with a minimum of two effective intermediates that require rate coefficients to be tuned in addition to all yields; thus, the uncertainty for modeling the pH 2 data is much higher. In addition, the model reactions at pH 2 cannot be easily mapped to physical reactions. The total gross production yield for the volatile acids from all generations can be roughly estimated as ∼2 for formate and ∼0.5 for acetate at pH 9. At pH 2, the gross production yield is 2−3 for FA and 1.5−2 for AA after applying the partitioning correction range shown in Table 1. These gross production yields are high and account for the majority of carbons in 2-MT within uncertainty.

Atmospheric Relevance and Conclusions. We demonstrated that the aqueous hydroxyl-radical-initiated oxidation of 2-methyltetrol produces mainly formic acid, acetic acid, and CO_2 at nearly quantitative yields. The photochemical loss of 2-MT is significant but not yet considered in many atmospheric models. As recent updates to global models have tended to overestimate total isoprene SOA, the consideration of this sink for 2-MT may be helpful for models to more accurately reproduce observations.[30−32] The observed concentrations of FA and AA in solution will be affected by pH, which affects their gas−aqueous partitioning, gross production yields via controlling the fate of RO_2 radicals derived from 2-MT, and radical-induced oxidation. At strongly or mildly acidic pH, which is most relevant to atmospheric water phases, partitioning to the gas phase will be a major fate of the small acids, which may contribute to the "missing" formic and acetic acid emission fluxes in biogenic areas. The additional methyl group of 2-methyltetrol drastically changes the chemistry of the oxidation reaction compared to erythritol, such that the formation of volatile acids is more prompt, even though the kinetics of the polyol decay occurs more slowly. RO_2 and RO reactions appear to be highly important in the aqueous phase, and the RO_2 fate is sensitive to solution pH, suggesting a need to study the fate of these radicals in water to supplement knowledge gaps in the literature. Further work is needed to quantify the yields of small acids, in both the aerosol and gas phase, from suitable SOA constituents in bulk solutions and on suspended particles to gain a better chemical understanding of small acid formation in atmospheric aqueous phases.

■ ASSOCIATED CONTENT

Supporting Information

The Supporting Information is available free of charge at https://pubs.acs.org/doi/10.1021/acsearthspacechem.1c00107.

> Emission flux from an UV lamp, kinetic decay of 2-MT quantified by LC−MS and NMR, expanded view of ^{13}C NMR data, all identified signals in HPLC−MS for the photooxidation of 2-erythritol and 2-methyltetrol, proposed mechanism for glycolic acid photooxidation, and kinetic model mechanism at pH 2 and 9 (PDF)

■ AUTHOR INFORMATION

Corresponding Author

Tran B. Nguyen − *Department of Environmental Toxicology, University of California, Davis, Davis, California 95616, United States;* orcid.org/0000-0001-9206-4359; Email: tbn@ucdavis.edu

Authors

James D. Cope − *Department of Environmental Toxicology, University of California, Davis, Davis, California 95616, United States;* orcid.org/0000-0002-0917-0730

Karizza A. Abellar − *Department of Chemistry, University of California, Davis, Davis, California 95616, United States*

Kelvin H. Bates − *Department of Environmental Toxicology, University of California, Davis, Davis, California 95616, United States; Center for the Environment, Harvard University, Cambridge, Massachusetts 02138, United States;* orcid.org/0000-0001-7544-9580

Xuan Fu − *Department of Environmental Toxicology, University of California, Davis, Davis, California 95616, United States*

Complete contact information is available at:

https://doi.org/10.1021/acsearthspacechem.1c00107
ACS Earth Space Chem. XXXX, XXX, XXX−XXX

https://pubs.acs.org/10.1021/acsearthspacechem.1c00107

Funding

The authors acknowledge funding from the National Science Foundation Atmospheric Chemistry Program under Grant AGS-1656889 and the California Agricultural Experiment Station Grant CAD-ETX-2345-H through the United States Department of Agriculture (USDA) National Institute of Food and Agriculture. Funding for the 400 MHz Advance III was provided by the National Science Foundation (9808183) and National Institute of Health [ES005707-13 (BACS 60)].

Notes

The authors declare no competing financial interest.

REFERENCES

(1) Khare, P.; Kumar, N.; Kumari, K. M.; Srivastava, S. S. Atmospheric formic and acetic acids: An overview. *Rev. Geophys.* **1999**, *37* (2), 227.

(2) Yu, S. C. Role of organic acids (formic, acetic, pyruvic and oxalic) in the formation of cloud condensation nuclei (CCN): A review. *Atmos. Res.* **2000**, *53* (4), 185.

(3) Wang, S.; Newland, M. J.; Deng, W.; Rickard, A. R.; Hamilton, J. F.; Munoz, A.; Rodenas, M.; Vazquez, M. M.; Wang, L.; Wang, X. Aromatic Photo-oxidation, A New Source of Atmospheric Acidity. *Environ. Sci. Technol.* **2020**, *54* (13), 7798.

(4) Andreae, M. O.; Talbot, R. W.; Andreae, T. W.; Harriss, R. C. Formic and Acetic-Acid over the Central Amazon Region, Brazil.1. Dry Season. *J. Geophys. Res.* **1988**, *93* (D2), 1616.

(5) Stavrakou, T.; Müller, J-F.; Peeters, J.; Razavi, A.; Clarisse, L.; Clerbaux, C.; Coheur, P-F.; Hurtmans, D.; De Mazière, M.; Vigouroux, C.; Deutscher, N. M.; Griffith, D. W. T.; Jones, N.; Paton-Walsh, C. Satellite evidence for a large source of formic acid from boreal and tropical forests. *Nat. Geosci.* **2012**, *5* (1), 26.

(6) Paulot, F.; Wunch, D.; Crounse, J. D.; Toon, G. C.; Millet, D. B.; DeCarlo, P. F.; Vigouroux, C.; Deutscher, N. M.; González Abad, G.; Notholt, J.; Warneke, T.; Hannigan, J. W.; Warneke, C.; de Gouw, J. A.; Dunlea, E. J.; De Mazière, M.; Griffith, D. W. T.; Bernath, P.; Jimenez, J. L.; Wennberg, P. O. Importance of secondary sources in the atmospheric budgets of formic and acetic acids. *Atmos. Chem. Phys.* **2011**, *11* (5), 1989.

(7) Chen, X.; Millet, D. B.; Singh, H. B.; Wisthaler, A.; Apel, E. C.; Atlas, E. L.; Blake, D. R.; Bourgeois, I.; Brown, S. S.; Crounse, J. D.; de Gouw, J. A.; Flocke, F. M.; Fried, A.; Heikes, B. G.; Hornbrook, R. S.; Mikoviny, T.; Min, K.-E.; Müller, M.; Neuman, J. A.; O'Sullivan, D. W.; Peischl, J.; Pfister, G. G.; Richter, D.; Roberts, J. M.; Ryerson, T. B.; Shertz, S. R.; Thompson, C. R.; Treadaway, V.; Veres, P. R.; Walega, J.; Warneke, C.; Washenfelder, R. A.; Weibring, P.; Yuan, B. On the sources and sinks of atmospheric VOCs: An integrated analysis of recent aircraft campaigns over North America. *Atmos. Chem. Phys.* **2019**, *19* (14), 9097.

(8) Mungall, E. L.; Abbatt, J. P. D.; Wentzell, J. J. B.; Lee, A. K. Y.; Thomas, J. L.; Blais, M.; Gosselin, M.; Miller, L. A.; Papakyriakou, T.; Willis, M. D.; Liggio, J. Microlayer source of oxygenated volatile organic compounds in the summertime marine Arctic boundary layer. *Proc. Natl. Acad. Sci. U. S. A.* **2017**, *114* (24), 6203.

(9) Millet, D. B.; Baasandorj, M.; Farmer, D. K.; Thornton, J. A.; Baumann, K.; Brophy, P.; Chaliyakunnel, S.; de Gouw, J. A.; Graus, M.; Hu, L.; Koss, A.; Lee, B. H.; Lopez-Hilfiker, F. D.; Neuman, J. A.; Paulot, F.; Peischl, J.; Pollack, I. B.; Ryerson, T. B.; Warneke, C.; Williams, B. J.; Xu, J. A large and ubiquitous source of atmospheric formic acid. *Atmos. Chem. Phys.* **2015**, *15* (11), 6283.

(10) Schobesberger, S.; Lopez-Hilfiker, F. D.; Taipale, D.; Millet, D. B.; D'Ambro, E. L.; Rantala, P.; Mammarella, I.; Zhou, P.; Wolfe, G. M.; Lee, B. H.; Boy, M.; Thornton, J. A. High upward fluxes of formic acid from a boreal forest canopy. *Geophys. Res. Lett.* **2016**, *43* (17), 9342.

(11) Yuan, B.; Veres, P. R.; Warneke, C.; Roberts, J. M.; Gilman, J. B.; Koss, A.; Edwards, P. M.; Graus, M.; Kuster, W. C.; Li, S.-M.; Wild, R. J.; Brown, S. S.; Dubé, W. P.; Lerner, B. M.; Williams, E. J.; Johnson, J. E.; Quinn, P. K.; Bates, T. S.; Lefer, B.; Hayes, P. L.; Jimenez, J. L.; Weber, R. J.; Zamora, R.; Ervens, B.; Millet, D. B.; Rappenglück, B.; de Gouw, J. A. Investigation of secondary formation of formic acid: Urban environment vs. oil and gas producing region. *Atmos. Chem. Phys.* **2015**, *15* (4), 1975.

(12) von Kuhlmann, R. A model for studies of tropospheric ozone and nonmethane hydrocarbons: Model evaluation of ozone-related species. *J. Geophys. Res.* **2003**, *108* (D23), 4729.

(13) Link, M. F.; Nguyen, T. B.; Bates, K.; Müller, J.-F.; Farmer, D. K. Can Isoprene Oxidation Explain High Concentrations of Atmospheric Formic and Acetic Acid over Forests? *ACS Earth Space Chem.* **2020**, *4* (5), 730.

(14) Liggio, J.; Moussa, S. G.; Wentzell, J.; Darlington, A.; Liu, P.; Leithead, A.; Hayden, K.; O'Brien, J.; Mittermeier, R. L.; Staebler, R.; Wolde, M.; Li, S.-M. Understanding the primary emissions and secondary formation of gaseous organic acids in the oil sands region of Alberta, Canada. *Atmos. Chem. Phys.* **2017**, *17* (13), 8411.

(15) Paulot, F.; Crounse, J. D.; Kjaergaard, H. G.; Kurten, A.; St. Clair, J. M.; Seinfeld, J. H.; Wennberg, P. O. Unexpected epoxide formation in the gas-phase photooxidation of isoprene. *Science* **2009**, *325* (5941), 730.

(16) St. Clair, J. M.; Rivera-Rios, J. C.; Crounse, J. D.; Knap, H. C.; Bates, K. H.; Teng, A. P.; Jørgensen, S.; Kjaergaard, H. G.; Keutsch, F. N.; Wennberg, P. O. Kinetics and Products of the Reaction of the First-Generation Isoprene Hydroxy Hydroperoxide (ISOPOOH) with OH. *J. Phys. Chem. A* **2016**, *120* (9), 1441.

(17) Kleindienst, T. E.; Lewandowski, M.; Offenberg, J. H.; Jaoui, M.; Edney, E. O. The formation of secondary organic aerosol from the isoprene plus OH reaction in the absence of NOx. *Atmos. Chem. Phys.* **2009**, *9* (17), 6541.

(18) Nguyen, T. B.; Coggon, M. M.; Bates, K. H.; Zhang, X.; Schwantes, R. H.; Schilling, K. A.; Loza, C. L.; Flagan, R. C.; Wennberg, P. O.; Seinfeld, J. H. Organic aerosol formation from the reactive uptake of isoprene epoxydiols (IEPOX) onto non-acidified inorganic seeds. *Atmos. Chem. Phys.* **2014**, *14* (7), 3497.

(19) Surratt, J.; Chan, A. W. H.; Eddingsaas, N. C.; Chan, M.; Loza, C. L.; Kwan, A. J.; Hersey, S. P.; Flagan, R. C.; Wennberg, P. O.; Seinfeld, J. H. Reactive intermediates revealed in secondary organic aerosol formation from isoprene. *Proc. Natl. Acad. Sci. U. S. A.* **2010**, *107*, 6640.

(20) Claeys, M.; Wang, W.; Ion, A. C.; Kourtchev, I.; Gelencser, A.; Maenhaut, W. Formation of secondary organic aerosols from isoprene and its gas-phase oxidation products through reaction with hydrogen peroxide. *Atmos. Environ.* **2004**, *38* (25), 4093.

(21) Kourtchev, I.; Ruuskanen, T.; Maenhaut, W.; Kulmala, M.; Claeys, M. Observation of 2-methyltetrols and related photo-oxidation products of isoprene in boreal forest aerosols from Hyytiälä, Finland. *Atmos. Chem. Phys.* **2005**, *5* (10), 2761.

(22) Liang, L. L.; Engling, G.; Duan, F. K.; Cheng, Y.; He, K. B. Characteristics of 2-methyltetrols in ambient aerosol in Beijing, China. *Atmos. Environ.* **2012**, *59*, 376.

(23) Hughes, D. D.; Christiansen, M. B.; Milani, A.; Vermeuel, M. P.; Novak, G. A.; Alwe, H. D.; Dickens, A. F.; Pierce, R. B.; Millet, D. B.; Bertram, T. H.; Stanier, C. O.; Stone, E. A. $PM_{2.5}$ chemistry, organosulfates, and secondary organic aerosol during the 2017 Lake Michigan Ozone Study. *Atmos. Environ.* **2021**, *244*, 117939.

(24) Clements, A. L.; Seinfeld, J. H. Detection and quantification of 2-methyltetrols in ambient aerosol in the southeastern United States. *Atmos. Environ.* **2007**, *41* (9), 1825.

(25) Karambelas, A.; Pye, H. O. T.; Budisulistiorini, S. H.; Surratt, J. D.; Pinder, R. W. Contribution of Isoprene Epoxydiol to Urban Organic Aerosol: Evidence from Modeling and Measurements. *Environ. Sci. Technol. Lett.* **2014**, *1* (6), 278.

(26) Chan, M. N.; Surratt, J. D.; Claeys, M.; Edgerton, E. S.; Tanner, R. L.; Shaw, S. L.; Zheng, M.; Knipping, E. M.; Eddingsaas, N. C.; Wennberg, P. O.; Seinfeld, J. H. Characterization and quantification

of isoprene-derived epoxydiols in ambient aerosol in the southeastern United States. *Environ. Sci. Technol.* **2010**, *44* (12), 4590.
(27) Pye, H. O. T.; Pinder, R. W.; Piletic, I. R.; Xie, Y.; Capps, S. L.; Lin, Y.-H.; Surratt, J. D.; Zhang, Z.; Gold, A.; Luecken, D. J.; Hutzell, W. T.; Jaoui, M.; Offenberg, J. H.; Kleindienst, T. E.; Lewandowski, M.; Edney, E. O. Epoxide pathways improve model predictions of isoprene markers and reveal key role of acidity in aerosol formation. *Environ. Sci. Technol.* **2013**, *47*, 11056.
(28) Ding, X.; Zheng, M.; Yu, L.; Zhang, X.; Weber, R. J.; Yan, B.; Russell, A. G.; Edgerton, E. S.; Wang, X. Spatial and Seasonal Trends in Biogenic Secondary Organic Aerosol Tracers and Water-Soluble Organic Carbon in the Southeastern United States. *Environ. Sci. Technol.* **2008**, *42* (14), 5171.
(29) Lin, Y. H.; Knipping, E. M.; Edgerton, E. S.; Shaw, S. L.; Surratt, J. D. Investigating the influences of SO_2 and NH_3 levels on isoprene-derived secondary organic aerosol formation using conditional sampling approaches. *Atmos. Chem. Phys.* **2013**, *13* (16), 8457.
(30) Stadtler, S.; Kühn, T.; Schröder, S.; Taraborrelli, D.; Schultz, M. G.; Kokkola, H. Isoprene-derived secondary organic aerosol in the global aerosol-chemistry-climate model ECHAM6.3.0-HAM2.3-MOZ1.0. *Geosci. Model Dev.* **2018**, *11* (8), 3235.
(31) Bates, K. H.; Jacob, D. J. A new model mechanism for atmospheric oxidation of isoprene: Global effects on oxidants, nitrogen oxides, organic products, and secondary organic aerosol. *Atmos. Chem. Phys.* **2019**, *19* (14), 9613.
(32) Hodzic, A.; Kasibhatla, P. S.; Jo, D. S.; Cappa, C. D.; Jimenez, J. L.; Madronich, S.; Park, R. J. Rethinking the global secondary organic aerosol (SOA) budget: Stronger production, faster removal, shorter lifetime. *Atmos. Chem. Phys.* **2016**, *16* (12), 7917.
(33) Nguyen, T. K. V.; Petters, M. D.; Suda, S. R.; Guo, H.; Weber, R. J.; Carlton, A. G. Trends in particle-phase liquid water during the Southern Oxidant and Aerosol Study. *Atmos. Chem. Phys.* **2014**, *14* (20), 10911.
(34) Gerber, H. Liquid Water-Content of Fogs and Hazes from Visible-Light Scattering. *J. Clim. Appl. Meteorol.* **1984**, *23* (8), 1247.
(35) Reid, J. S.; Hobbs, P. V.; Rangno, A. L.; Hegg, D. A. Relationships between cloud droplet effective radius, liquid water content, and droplet concentration for warm clouds in Brazil embedded in biomass smoke. *J. Geophys. Res. Atmos.* **1999**, *104* (D6), 6145.
(36) Herrmann, H.; Hoffmann, D.; Schaefer, T.; Brauer, P.; Tilgner, A. Tropospheric aqueous-phase free-radical chemistry: Radical sources, spectra, reaction kinetics and prediction tools. *ChemPhysChem* **2010**, *11* (18), 3796.
(37) Daumit, K. E.; Carrasquillo, A. J.; Hunter, J. F.; Kroll, J. H. Laboratory studies of the aqueous-phase oxidation of polyols: Submicron particles vs. bulk aqueous solution. *Atmos. Chem. Phys.* **2014**, *14* (19), 10773.
(38) Zhao, R.; Lee, A.; Wang, C.; Wania, F.; Wong, J.; Zhou, S.; Abbatt, J. The role of water in organic aerosol multiphase chemistry: Focus on partitioning and reactivity. *Adv. Atmos. Chem.* **2017**, 95.
(39) Herrmann, H.; Schaefer, T.; Tilgner, A.; Styler, S. A.; Weller, C.; Teich, M.; Otto, T. Tropospheric aqueous-phase chemistry: Kinetics, mechanisms, and its coupling to a changing gas phase. *Chem. Rev.* **2015**, *115* (10), 4259.
(40) McNeill, V. F. Aqueous organic chemistry in the atmosphere: Sources and chemical processing of organic aerosols. *Environ. Sci. Technol.* **2015**, *49* (3), 1237.
(41) Sareen, N.; Carlton, A. G.; Surratt, J. D.; Gold, A.; Lee, B.; Lopez-Hilfiker, F. D.; Mohr, C.; Thornton, J. A.; Zhang, Z.; Lim, Y. B.; Turpin, B. J. Identifying precursors and aqueous organic aerosol formation pathways during the SOAS campaign. *Atmos. Chem. Phys.* **2016**, *16* (22), 14409.
(42) Fahey, K. M.; Carlton, A. G.; Pye, H. O. T.; Baek, J.; Hutzell, W. T.; Stanier, C. O.; Baker, K. R.; Appel, K. W.; Jaoui, M.; Offenberg, J. H. A framework for expanding aqueous chemistry in the Community Multiscale Air Quality (CMAQ) model version 5.1. *Geosci. Model Dev.* **2017**, *10* (4), 1587.
(43) Marais, E. A.; Jacob, D. J.; Jimenez, J. L.; Campuzano-Jost, P.; Day, D. A.; Hu, W.; Krechmer, J.; Zhu, L.; Kim, P. S.; Miller, C. C.; Fisher, J. A.; Travis, K.; Yu, K.; Hanisco, T. F.; Wolfe, G. M.; Arkinson, H. L.; Pye, H. O. T.; Froyd, K. D.; Liao, J.; McNeill, V. F. Aqueous-phase mechanism for secondary organic aerosol formation from isoprene: Application to the Southeast United States and co-benefit of SO_2 emission controls. *Atmos. Chem. Phys.* **2016**, *16* (3), 1603.
(44) Kirkland, J. R.; Lim, Y. B.; Tan, Y.; Altieri, K. E.; Turpin, B. J. Glyoxal secondary organic aerosol chemistry: Effects of dilute nitrate and ammonium and support for organic radical-radical oligomer formation. *Environ. Chem.* **2013**, *10* (3), 158.
(45) Tan, Y.; Perri, M. J.; Seitzinger, S. P.; Turpin, B. J. Effects of precursor concentration and acidic sulfate in aqueous glyoxal-OH radical oxidation and implications for secondary organic aerosol. *Environ. Sci. Technol.* **2009**, *43* (21), 8105.
(46) Lee, A. K. Y.; Herckes, P.; Leaitch, W. R.; Macdonald, A. M.; Abbatt, J. P. D. Aqueous OH oxidation of ambient organic aerosol and cloud water organics: Formation of highly oxidized products. *Geophys. Res. Lett.* **2011**, *38* (11), 11805.
(47) McNeill, V. F.; Woo, J. L.; Kim, D. D.; Schwier, A. N.; Wannell, N. J.; Sumner, A. J.; Barakat, J. M. Aqueous-phase secondary organic aerosol and organosulfate formation in atmospheric aerosols: A modeling study. *Environ. Sci. Technol.* **2012**, *46* (15), 8075.
(48) Liu, M. J.; Wiegel, A. A.; Wilson, K. R.; Houle, F. A. Aerosol Fragmentation Driven by Coupling of Acid-Base and Free-Radical Chemistry in the Heterogeneous Oxidation of Aqueous Citric Acid by OH Radicals. *J. Phys. Chem. A* **2017**, *121* (31), 5856.
(49) Bondy, A. L.; Craig, R. L.; Zhang, Z.; Gold, A.; Surratt, J. D.; Ault, A. P. Isoprene-Derived Organosulfates: Vibrational Mode Analysis by Raman Spectroscopy, Acidity-Dependent Spectral Modes, and Observation in Individual Atmospheric Particles. *J. Phys. Chem. A* **2018**, *122* (1), 303.
(50) Zwiener, C.; Glauner, T.; Frimmel, F. H. Method optimization for the determination of carbonyl compounds in disinfected water by DNPH derivatization and LC−ESI−MS−MS. *Anal. Bioanal. Chem.* **2002**, *372* (5−6), 615.
(51) Li, Y.; Burns, A. E.; Burke, G. J. P.; Poindexter, M. E.; Madl, A. K.; Pinkerton, K. E.; Nguyen, T. B. Application of High-Resolution Mass Spectrometry and a Theoretical Model to the Quantification of Multifunctional Carbonyls and Organic Acids in e-Cigarette Aerosol. *Environ. Sci. Technol.* **2020**, *54* (9), 5640.
(52) Chatterjee, T.; Boutin, E.; Robert, M. Manifesto for the routine use of NMR for the liquid product analysis of aqueous CO_2 reduction: From comprehensive chemical shift data to formaldehyde quantification in water. *Dalton Trans* **2020**, *49* (14), 4257.
(53) Rivlin, M.; Eliav, U.; Navon, G. NMR studies of the equilibria and reaction rates in aqueous solutions of formaldehyde. *J. Phys. Chem. B* **2015**, *119* (12), 4479.
(54) Fulmer, G. R.; Miller, A. J. M.; Sherden, N. H.; Gottlieb, H. E.; Nudelman, A.; Stoltz, B. M.; Bercaw, J. E.; Goldberg, K. I. NMR Chemical Shifts of Trace Impurities: Common Laboratory Solvents, Organics, and Gases in Deuterated Solvents Relevant to the Organometallic Chemist. *Organometallics* **2010**, *29* (9), 2176.
(55) Abellar, K. A.; Cope, J. D.; Nguyen, T. B. Second-order kinetic rate coefficients for the aqueous-phase hydroxyl radical (OH) oxidation of isoprene-derived secondary organic aerosol compounds at 298 K. Manuscript in preparation.
(56) Tynkkynen, T.; Tiainen, M.; Soininen, P.; Laatikainen, R. From proton nuclear magnetic resonance spectra to pH. Assessment of 1H NMR pH indicator compound set for deuterium oxide solutions. *Anal. Chim. Acta* **2009**, *648* (1), 105.
(57) Erdemgil, F. Z.; Sanli, S.; Sanli, N.; Ozkan, G.; Barbosa, J.; Guiteras, J.; Beltran, J. L. Determination of pK(a) values of some hydroxylated benzoic acids in methanol-water binary mixtures by LC methodology and potentiometry. *Talanta* **2007**, *72* (2), 489.
(58) Chin, M.; Wine, P. H. A Temperature-Dependent Competitive Kinetics Study of the Aqueous-Phase Reactions of OH Radicals with Formate, Formic Acid, Acetate, Acetic Acid, and Hydrated Form-

https://doi.org/10.1021/acsearthspacechem.1c00107
ACS Earth Space Chem. XXXX, XXX, XXX−XXX

aldehyde. In *Aquatic and Surface Photochemistry*; Heiz, G. R., Zepp, R. G., Crosby, D. G., Eds.; CRC Press: Boca Raton, FL, 1994; Chapter 5, p 85, DOI: 10.1201/9781351069847-6.
(59) Palmer, D. A.; Drummond, S. E. Thermal decarboxylation of acetate. Part I. The kinetics and mechanism of reaction in aqueous solution. *Geochim. Cosmochim. Acta* **1986**, *50* (5), 813.
(60) Concia, A. L.; Lozano, C.; Castillo, J. A.; Parella, T.; Joglar, J.; Clapes, P. D-fructose-6-phosphate aldolase in organic synthesis: Cascade chemical-enzymatic preparation of sugar-related polyhydroxylated compounds. *Chem. - Eur. J.* **2009**, *15* (15), 3808.
(61) Bose, S.; Wijeratne, A. B.; Thite, A.; Kraus, G. A.; Armstrong, D. W.; Petrich, J. W. Influence of chiral ionic liquids on stereoselective fluorescence quenching by photoinduced electron transfer in a naproxen dyad. *J. Phys. Chem. B* **2009**, *113* (31), 10825.
(62) Aganov, A. V.; Antonovskii, V. L. 13C NMR Spectra of organic peroxides. *Bull. Acad. Sci. USSR, Div. Chem. Sci.* **1982**, *31* (2), 247.
(63) Asmus, C.; Mozziconacci, O.; Schoneich, C. Low-temperature NMR characterization of reaction of sodium pyruvate with hydrogen peroxide. *J. Phys. Chem. A* **2015**, *119* (6), 966.
(64) Wennberg, P. O.; Bates, K. H.; Crounse, J. D.; Dodson, L. G.; McVay, R. C.; Mertens, L. A.; Nguyen, T. B.; Praske, E.; Schwantes, R. H.; Smarte, M. D.; St. Clair, J. M.; Teng, A. P.; Zhang, X.; Seinfeld, J. H. Gas-Phase Reactions of Isoprene and Its Major Oxidation Products. *Chem. Rev.* **2018**, *118* (7), 3337.
(65) Teng, A. P.; Crounse, J. D.; Wennberg, P. O. Isoprene Peroxy Radical Dynamics. *J. Am. Chem. Soc.* **2017**, *139* (15), 5367.
(66) Asmus, K.; Möckel, H.; Henglein, A. Pulse radiolytic study of the site of hydroxyl radical attack on aliphatic alcohols in aqueous solution. *J. Phys. Chem.* **1973**, *77* (10), 1218.
(67) Yang, L. H.; Li, X. W.; Chen, P.; Hou, Z. Y. Selective oxidation of glycerol in a base-free aqueous solution: A short review. *Chin. J. Catal.* **2019**, *40* (7), 1020.
(68) Van Haasterecht, T.; Van Deelen, T.; De Jong, K.; Bitter, J. Transformations of polyols to organic acids and hydrogen in aqueous alkaline media. *Catal. Sci. Technol.* **2014**, *4* (8), 2353.
(69) Carter, W. P.; Darnall, K. R.; Graham, R. A.; Winer, A. M.; Pitts, J. N. Reactions of C2 and C4. alpha.-hydroxy radicals with oxygen. *J. Phys. Chem.* **1979**, *83* (18), 2305.
(70) Xujia, Z.; Jilan, W.; Yurong, Z. The reaction of alpha-hydroxyethyl radical in aqueous solution and ethyl alcohol. *Radiat. Phys. Chem.* **1994**, *43* (4), 335.
(71) Wagner, P. J.; Zhang, Y.; Puchalski, A. E. Rate Constants for Degenerate Hydrogen-Atom Exchange between Alpha-Hydroxy Radicals and Ketones. *J. Phys. Chem.* **1993**, *97* (50), 13368.
(72) Oyama, M. A Free-Radical Reaction of Primary and Secondary Alcohols with Formaldehyde. *J. Org. Chem.* **1965**, *30* (7), 2429.
(73) Ilan, Y.; Rabani, J.; Henglein, A. Pulse Radiolytic Investigations of Peroxy Radicals Produced from 2-Propanol and Methanol. *J. Phys. Chem.* **1976**, *80* (14), 1558.
(74) Bothe, E.; Behrens, G.; Schulte-Frohlinde, D. Mechanism of the First Order Decay of 2-Hydroxy-propyl-2-peroxyl Radicals and of O_2^- Formation in Aqueous Solution. *Z. Naturforsch., B: J. Chem. Sci.* **1977**, *32* (8), 886.
(75) Bothe, E.; Schultefrohlinde, D. Reaction of Dihydroxymethyl Radical with Molecular-Oxygen in Aqueous-Solution. *Z. Naturforsch., B: J. Chem. Sci.* **1980**, *35* (8), 1035.
(76) Bothe, E.; Schulte-Frohlinde, D.; von Sonntag, C. Radiation chemistry of carbohydrates. Part 16. Kinetics of $HO_2^{\cdot}$ elimination from peroxyl radicals derived from glucose and polyhydric alcohols. *J. Chem. Soc., Perkin Trans. 2* **1978**, No. 5, 416.
(77) Shivers, R. R. Formation of junctional complexes at sites of contact of hemocytes with tissue elements in degenerating nerves of the crayfish, Orconectes virilis. *Tissue Cell* **1977**, *9* (1), 43.
(78) Finlayson-Pitts, B. J.; Pitts, J. N. *Chemistry of the Upper and Lower Atmosphere: Theory, Experiments, and Applications*; Academic Press: San Diego, CA, 2000; DOI: 10.1016/B978-0-12-257060-5.X5000-X.
(79) Kochi, J. K. Chemistry of Alkoxy Radicals—Cleavage Reactions. *J. Am. Chem. Soc.* **1962**, *84* (7), 1193.
(80) Bothe, E.; Schuchmann, M. N.; Schulte-Frohlinde, D.; Sonntag, C. v. HO_2 elimination from α-hydroxyalkylperoxyl radicals in aqueous solution. *Photochem. Photobiol.* **1978**, *28* (4−5), 639.
(81) Mulazzani, Q. G.; D'Angelantonio, M.; Venturi, M.; Hoffman, M. Z.; Rodgers, M. A. J. Interaction of Formate and Oxalate Ions with Radiation-Generated Radicals in Aqueous Solution. Methylviologen as a Mechanistic Probe. *J. Phys. Chem.* **1986**, *90* (21), 5347.
(82) Bielski, B. H. J.; Cabelli, D. E.; Arudi, R. L.; Ross, A. B. Reactivity of perhydroxyl/superoxide radicals in aqueous solution. *J. Phys. Chem. Ref. Data* **1985**, *14* (4), 1041.
(83) Haag, W. R.; Yao, C. D. Rate constants for reaction of hydroxyl radicals with several drinking water contaminants. *Environ. Sci. Technol.* **1992**, *26* (5), 1005.

https://doi.org/10.1021/acsearthspacechem.1c00107
ACS Earth Space Chem. XXXX, XXX, XXX−XXX